Annual Reports A

View Online Dynamic Article Links

Cite this: *Annu. Rep. Prog. Chem., Sect. A*, 2011, **107**, 419–433

www.rsc.org/annrepa

REVIEW

New compounds and structures in the solid state

Edmund J. Cussen

DOI: 10.1039/c1ic90028e

This chapter reviews the 2010 literature on new compounds and structures in the solid state.

Highlights

Highlights from the 2010 literature span the full range of compositions and properties that can be observed in continuous framework solids. Polymorphism in Cs_3C_{60} has allowed a decoupling of the factors that determine the superconducting transition temperature and concluded that these are independent of the lattice type.[1] The use of ionic liquids as a solvent for chalcogenides has resulted in the discovery of a porous intermetallic phase that selectively exchanges Cs^+ from a mixed solution of cations and encapsulates it by a mechanism familiar from the Venus flytrap.[2] A polar polymorph has been found in a phase that is the parent to many technologically important piezoelectric materials.[3] A number of fascinating studies have observed interesting properties arising from manipulation of the anion sublattice including high ion conductivity,[4] unusual cation ordering schemes[5] and the stabilisation of highly reduced phases.[6]

1. Oxides

A number of studies have examined the impact of subtle structural effects on the organisation of electric dipoles in new oxides. $NaNbO_3$ is a well-studied compound that can be doped to give lead-free ceramics with excellent piezoelectric properties. A painstaking study of $NaNbO_3$ has found that in addition to the orthorhombic antiferroelectric phase previously reported in the literature it is possible to prepare a polar phase with a subtle monoclinic distortion in the space group $P2_1ma$ using sol–gel techniques.[3] These two polymorphs appear to have similar stabilities and mixed phase samples are often observed. The identification of phase pure samples requires detailed examination using a wide-range of probes in order to resolve the relatively subtle differences between the phases. Given the piezoelectric behaviour of

WestCHEM, Department of Pure and Applied Chemistry, The University of Strathclyde, Glasgow, Scotland, UK, G12 8PU. E-mail: EdmundCussen@Strath.ac.uk; Fax: +44 141 548 4822; Tel: +44 141 548 2797

related phases these structural subtleties are likely to be of great technological importance.

Improvements in piezoelectric performance have been found in lead-based perovskites by using a solution growth method to prepare crystals of approximate composition $PbYb_{0.075}Mg_{0.177}Nb_{0.428}Ti_{0.32}O_3$. The introduction of ytterbium into the structure raises both the Curie temperature and the coercive field necessary to depolarise the material. It is anticipated that the resultant material can operate over a wider temperature range up to the ordering temperature of 205 °C.[7] Interesting magnetic behaviour has been reported in the polar non-centrosymmetric phase $VOSe_2O_5$ which crystallises in the space group P4cc. This compound contains chains of VO_6 octahedra that are linked by Se_2O_5 groups composed of vertex-linked trigonal planar SeO_3 units as shown in Fig. 1.[8] These planar units arise from stereoactive lone pairs of electrons associated with the Se^{4+} cation and introduce polarity into the structure. This compound forms a ferrimagnetically ordered phase at 8 K and undergoes two further additional magnetic transitions on cooling to 5.5 K and 4 K. The absence of additional magnetic Bragg peaks suggests that the ferrimagnetic structure does not violate the symmetry of the crystallographic structure, but the weak magnetic scattering did not allow refinement of a magnetic structure. Although this compound contains both electric and magnetic dipoles it is not possible to switch the latter and so this phase cannot be considered a multiferroic material.

The hexagonal perovskite $Sr_5Ru_{4.1}O_{15}$ has been prepared as a single crystal using oxidising conditions and a pressure of 4 GPa.[9] This structure contains a mixture of

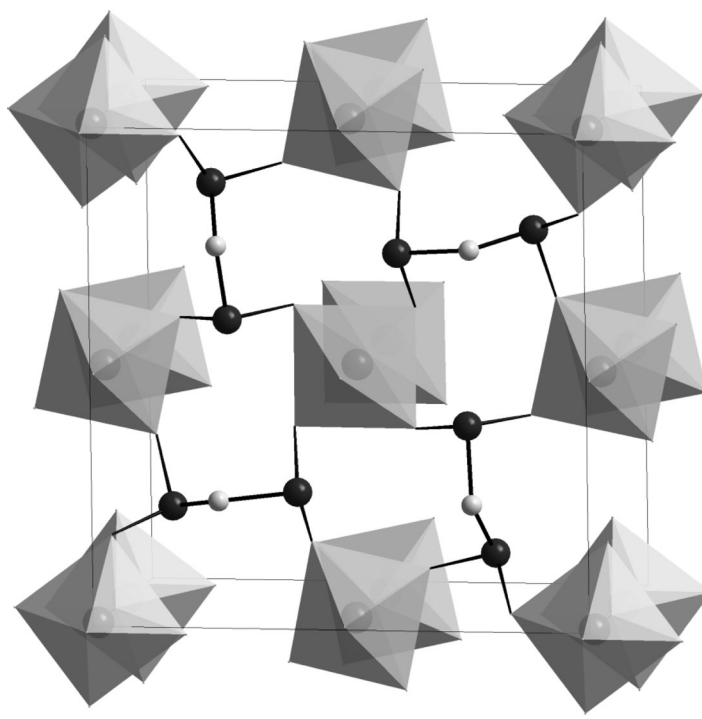

Fig. 1 The crystal structure of $VOSe_2O_5$. Octahedra represent VO_6 units and the black spheres represent selenium atoms in trigonal coordination.[8]

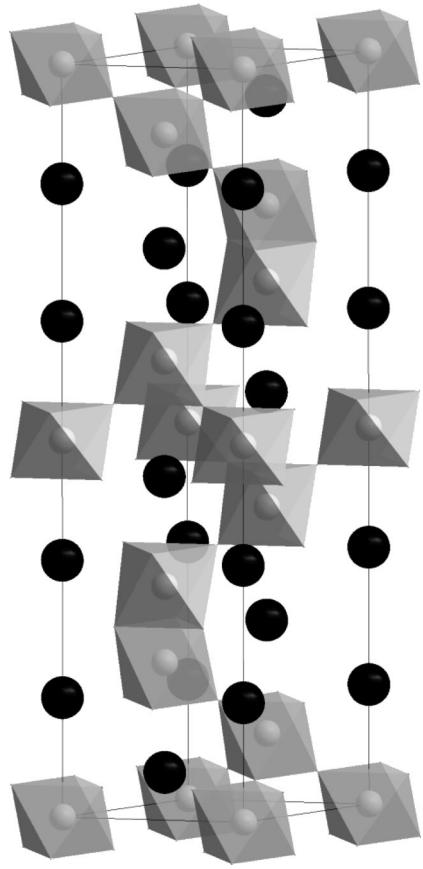

Fig. 2 The 10H structure of $Sr_5Ru_{5-x}O_{15}$ contains dimers of face-sharing RuO_6 octahedra linked by corner-sharing through a chain of three corners-sharing octahedra. Strontium cations are represented by black spheres.[9]

corner- and face-sharing RuO_6 in the structure with dimers of the latter being separated by three corner-linked octahedra. This leads to ten layers in the hexagonal unit cell and the 10H structure shown in Fig. 2. The non-stoichiometry is accommodated by ruthenium vacancies in the face-sharing octahedra and an increase in the mean oxidation state to $Ru^{4.87+}$. This compound displays metallic conductivity and a small magnetically ordered moment of *ca.* 0.06 μ_B per ruthenium cation below a magnetic transition temperature of 160 K. Whilst many of these observations can be understood with reference to known ruthenium perovskites, this compound is remarkable in showing a coercive field of 12 T. This is considerably larger than the materials currently employed as hard magnets and is the largest coercive field observed to date.

A series of rare-earth perovskites Ln_2MgIrO_6 have been prepared for the first time.[10] Interestingly, attempts to prepare these compounds using conventional high temperature methods failed to produce the target compounds as single phase samples. However, the use of a hydroxide flux produced single crystals suitable for diffraction experiments. All of these compounds adopt a monoclinically distorted perovskite structure with complete chemical ordering between the Mg^{2+} and Ir^{4+} cations. The size of the structural distortion progressively increases as the cation size is reduced from Nd^{3+} to Gd^{3+} and

it appears that heavier lanthanides with radii smaller than that of Gd^{3+} cannot be stabilised in these structures; the attempted syntheses of analogous compounds with lanthanide cations smaller than Gd^{3+} were unsuccessful. Pr_2MgIrO_6, Nd_2MgIrO_6, Sm_2MgIrO_6 and Eu_2MgIrO_6 all undergo antiferromagnetic transitions in the range $10 \leq T/K \leq 15$ whilst Gd_2MgIrO_6 remains paramagnetic to 2 K.

A number of new materials which form layered analogues of the perovskite structure have been reported. A series of compounds $La_{1.5+x}Sr_{0.5-x}Co_{0.5}Ni_{0.5}O_{4\pm\delta}$ have been prepared by varying the oxygen partial pressure during the synthesis.[11] These compounds contain a layer of perovskite separated by a single layer of rock salt structure. Oxygen deficiency is accommodated by vacancies within the Co/NiO_2 planes of the structure whilst excess oxide ions in $La_{1.7}Sr_{0.3}Co_{0.5}Ni_{0.5}O_{4.08}$ occupy interstitial sites between the layers without reducing the symmetry of the structure from I4/mmm. All compositions contain strong antiferromagnetic coupling and the oxygen rich compounds show semiconducting electrical conductivity of $\approx$ 100 S cm^{-1} that suggests that these may be useful as fuel cell materials. Analogous compounds $La_{1+x}Sr_{2-x}CoMnO_{7-\delta}$ contain a mixture of Co and Mn in a double layer of perovskite.[12] In the oxidised compounds these species are present as the Co^{3+}/Mn^{4+} couple and both cations are reduced to give Co^{2+}/Mn^{3+} in $LaSr_2CoMnO_6$ and $La_{1.2}Sr_{1.8}CoMnO_6$ prepared by heating the oxidised phases under reducing conditions. This reduction in oxide content leads to a change in coordination environment from octahedral, in the as-prepared compounds, to square-based pyramidal by removing the central oxide ion from the perovskite slab and so breaking the link between the two transition metal cations as shown in Fig. 3.

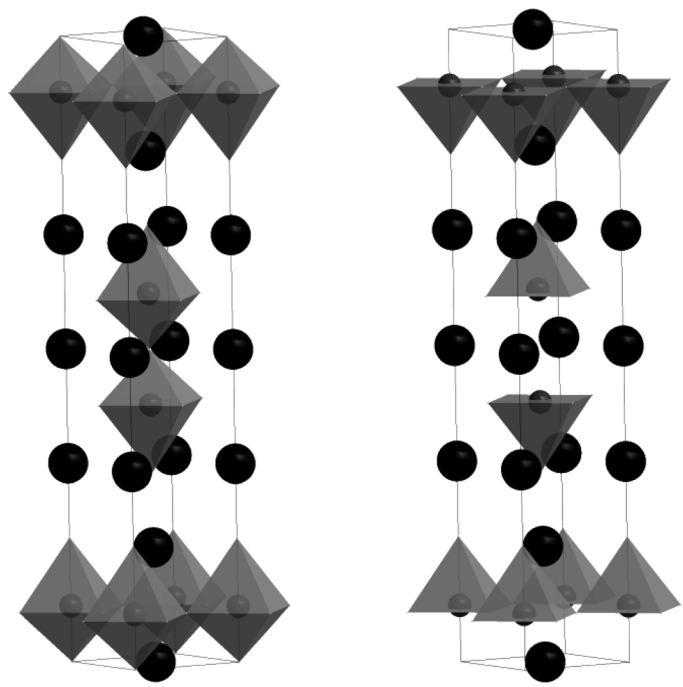

Fig. 3 The $n = 2$ Ruddlesden Popper structure of $A_3M_2O_{7-\delta}$. The oxidised phase contains a double perovskite layer (left). Reducing the phase removes the oxide from the middle of the perovskite slab and disrupts the connectivity (right). Polyhedra represent the transition metal coordination environment and black spheres represent A cations.[12]

This reduction changes the magnetic interactions from ferromagnetic to antiferromagnetic although disorder in these materials prevents the formation of a magnetically-ordered phase. A triple layer of perovskite is found in the new compound $NiClSr_2Ta_3O_{10}$[13] which is formed from a precursor compound $RbSr_2Ta_3O_{10}$ by reaction with $NiCl_2$ in a sealed evacuated pyrex tube at 340 °C. This procedure replaces Rb^+ with $(NiCl)^+$ whilst maintaining the perovskite block of $[Sr_2Ta_3O_{10}]^-$ leading to a tetragonal structure which shows considerable expansion in the interlayer region due to the increased size of $(NiCl)^+$ compared to Rb^+. The coupling between the Ni^{2+} cations is antiferromagnetic but this is substantially frustrated and leads to partial magnetic ordering at 50 K.

A detailed study of the brownmillerite Ca_2FeCoO_5 has identified unexpected cation ordering in this phase.[5] A combination of single crystal X-ray diffraction and powder neutron diffraction has shown that in addition to the relatively common ordering of cations across tetrahedral coordination sites there is also partial ordering within the octahedral sites. This is achieved in a unit cell which is doubled along one axis relative to most brownmillerites and so requires four different transition metal sites in the crystallographic unit cell. Coupling between the Fe^{3+} and Co^{3+} cations leads to long range G-type antiferromagnetic ordering with antiparallel coupling of adjacent moments. The orientation of the magnetic moments undergoes an unusual reorientation with the spins aligned along the [010] direction below 100 K gradually rotating until they are aligned along [100] at 200 K with some spin canting leading to an uncompensated bulk magnetic moment.

Anion vacancies in perovskites are coupled with ordering of larger cations in $YBaCo_2O_5$ and $LaBaCo_2O_5$ and the use of NaH as a solid state reducing agent on these compounds at relatively low temperatures has produced highly reduced phases $YBaCo_2O_{4.5}$ and $LaBaCo_2O_{4.25}$.[6] This extraction of oxide from the structure gives low coordination numbers for cobalt with distorted tetrahedral CoO_4 units and square-based pyramidal CoO_5 in $YBaCo_2O_{4.5}$ and an oxidation state of Co^{2+}. $LaBaCo_2O_{4.25}$ also shows both of these coordination environments but is further complicated by additional presence of CoO_4 in square planar geometry and the non-integer oxidation state $Co^{1.75+}$ arising from the presence of Co^+ in the square planar environment. This is the clearest observation of this oxidation state in an extended cobalt oxide.

Anion vacancies are responsible for the fast ion conductivity displayed by two new compounds that emulate the behaviour of δ-Bi_2O_3. $Bi_{25}La_3Re_2O_{49}$ and $Bi_{25}Pr_3Re_2O_{49}$ form face-centred cubic fluorite phases after synthesis at 800 °C and cooling to room temperature.[4] On subsequent heating, this phase transforms to a tetragonally-distorted variant of the structure with cation-ordering driving a distortion to a body-centred structure leading to a reduction in the oxide ion conductivity of two orders of magnitude. The rate of structural transformation is slow; it takes prolonged heating at 600 °C to transform from the cubic, conductive phase to the tetragonal, cation-ordered phase. At higher temperatures the tetragonal phase transforms back to the cubic disordered compound which is then stable on cooling to room temperature, providing another indication of the slow rate of order/disorder transformation. It is notable that the conductivity of the cation-ordered phases are considerably lower than the unsubstituted phase $Bi_{28}Re_2O_{49}$ and this suggests that the mechanism for oxide ion motion involves the oxide bonded to the site containing the lanthanide dopant. A fluorite-related structure has also been identified for the heterogeneous catalyst previously reported to have the composition Pr_2MoO_6. A neutron diffraction study showed an expanded unit cell that is barely detectable in the X-ray diffraction profile

and both data sets can be fitted using the cubic space group $Pn\bar{3}n$, $a = 11.08989(9)$ Å, and a stoichiometry $Pr_5Mo_3O_{16}$.[14] Detailed examination of the metal oxide bond lengths suggests that the Mo cations are slightly reduced to a mean oxidation state $Mo^{5.5+}$ and that Pr is present in a mixture of tri- and tetra-valent states. The doubling of the unit cell compared to the prototypical fluorite structure arises from the periodic substitution of PrO_8 units with MoO_4 tetrahedra. The ordering pattern leads to isolation of the MoO_4 tetrahedra and prevent the formation of electronically delocalised states often observed for partially reduced molybdates and so $Pr_5Mo_3O_{16}$ is electronically insulating at room temperature.

A series of partially lithiated phases Li_xTiO_2 have been studied using a combination of neutron diffraction and density functional theory in order to identify the sites for Li^+ in an polymorph of titanium dioxide formed by dehydration of the solid acid $H_2Ti_4O_9$ to give the phase TiO_2(B).[15] This phase contains TiO_6 octahedra linked by a mixture of corner- and edge-sharing. Electrochemical reductive insertion of small quantities of lithium into the structure to give an overall composition $Li_{0.15}TiO_2$ shows that the first site to be populated by lithium is a square planar coordination environment leading to a two phase sample containing a mixture of $Li_{0.25}TiO_2$(B) and TiO_2(B). Insertion of more than 0.25 Li^+ per TiO_2(B) unit leads to depopulation of the square planar lithium site and insertion instead onto a five-coordinate site. Increasing the lithium content up towards the maximum values of $Li_{0.8}TiO_2$(B) and $Li_{0.9}TiO_2$(B) for bulk and nanowire forms of the material leads to population of an additional five-coordinate site.

A series of compounds, *Ln*KNaTaO$_5$, have been prepared that contain unusual TaO_5 square pyramidal units.[16] The compounds are isostructural and contain layers composed of edge-sharing cubes of oxide anions which are 50% occupied by lanthanide cations in a rock salt arrangement. These layers are capped by TaO_5 units which are linked *via* corner-sharing between the square base of the TaO_5 unit and the top face of a vacant O_8 cube. Na and K are found between the layers in five- and twelve-coordinate sites respectively. This structure is unable to undergo distortion to reduce the coordination number of the lanthanide and this is thought to be responsible for the inability of this family of compounds to include the smaller lanthanides.

2. Oxyanions

New framework materials substantially composed of oxyanions have been found that display an exceptionally wide range of interesting properties. The framework hydroxide $Yb_3O(OH)_6Cl{\cdot}2H_2O$ contains one-dimensional channels in a three-dimensional array composed of positively charged ytterbium oxohydroxide built from oxide-centred Yb_4 tetrahedra linked by bridging hydroxide anions as shown in Fig. 4.[17] These channels contain a disordered mixture of water and chloride in the material that is prepared hydrothermally. The water can be removed by heating to give access to some of the 30% non-framework volume and this can be carried out reversibly at temperatures up to 200 °C with no loss of crystallinity. Treatment of the material with aqueous solutions containing other anions led to exchange for chloride and incorporation of species including carbonate, oxalate or succinate into the structure. This is the first time such ion-exchange behaviour has been reported in a hydroxide framework and combined with good thermal stability suggests that these phases may be the first of an important new family of porous materials. Another approach to producing three-dimensional structures from hydroxide frameworks is to use bi-dentate ligands to act as linkers between two-dimensional structures. This has led to a robust series of compounds where layered

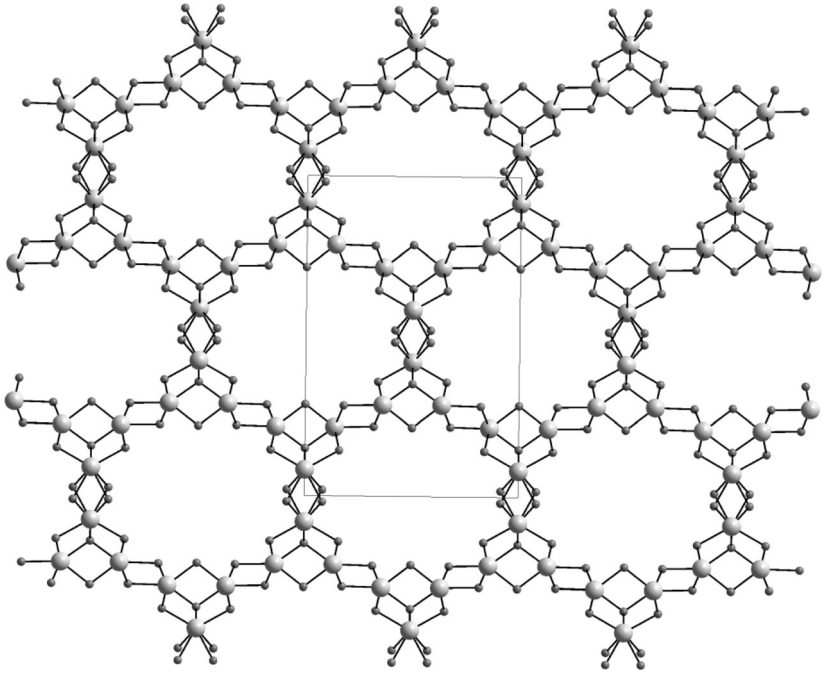

Fig. 4 The positively-charged framework of $Yb_3O(OH)_6Cl{\cdot}2H_2O$ is built up from Yb^{3+} cations shown as larger grey spheres and OH^- anions shown as smaller spheres.[17]

rare-earth hydroxide structures are pillared by sulfate to give $Ln_2(OH)_4SO_4{\cdot}nH_2O$; Ln = Pr to Tb and $n \approx 2$.[18] The sample was highly crystalline and the diffraction data could be indexed using a cell that indicated the presence of layers of lanthanide oxide whilst infra-red spectra showed the presence of sulfate as a *trans*-bidentate ligand. Heating these compounds to 450 °C leads to dehydration and the formation of the layered rare-earth oxysulfates $Ln_2O_2SO_4$ with a distinctive flake-like morphology.

A two-stage synthesis has been developed to give access to layered double hydroxides containing transition metal ions that are problematic in conventional synthesis of layered hydroxide. Brucite Co-Ni hydroxides, $Co_{2/3}Ni_{1/3}(OH)_2$, have been transformed using oxidative intercalation of bromine to give the mixed-valence compound $Co_{2/3}Ni_{1/3}Br_{1/3}(OH)_2$.[19] Carrying out control experiments on compounds containing either Co or Ni showed that the pure Ni compound is resistant to oxidation by bromine and suggests that the oxidative intercalation of a single bromine atom into the structure is associated with the oxidation of half of the cobalt ions to form Co^{3+}. Subsequent reactions can exchange a range of anions for Br^- due to the ability of the gap between the layers to vary without the sample losing crystallinity or can be exfoliated to give nanosheets. This synthetic approach thus gives access to a wide range of compounds which are likely to show interesting electronic properties due to the tuneable d-electron count.

The importance of this control is illustrated by the unusual magnetic behaviour that can be obtained in a simpler, mono-metallic hydroxide system. $K_2Co_3(OH)_2(SO_4)_3(H_2O)_2$ containing chains of CoO_6 octahedra linked *via* a combination of edge- and corner-sharing with sulfate ions linking the chains to give

a robust three-dimensional structure.[20] This material orders ferrimagnetically below 29.7 K with a saturated magnetisation of *ca.* 2.2 μ_B per formula unit which agrees well with the magnetic structure and indicates the magnetic moments of two Co^{2+} ions are aligned parallel to one another and antiparallel to the third, crystallographically distinct Co^{2+} ion. The magnetic hysteresis of this material is straightforward near the Curie temperature, but becomes highly anisotropic below 10 K with the coercive field along the *c* direction being the largest yet observed for a mineral structure type. It is thought that this arises from changes in the magnetic domain size and wall structure rather than single ion anisotropy arising from orbital effects.

Ferromagnetism is observed in the highly anisotropic material $VO(SeO_2OH)_2$.[21] This acentric compound contains chains of corner-sharing VO_6 octahedra linked by SeO_2OH groups and weak ferromagnetic coupling between the V^{4+} cations leads to ferromagnetic ordering at 2.5 K. This low ordering temperature results from competition between antiferro- and ferro-magnetic coupling that is extremely sensitive to the angle of the O-Se-O pathways that link the VO_6 chains. The stereoactive lone pair of electrons of Se^{4+} is a key component in driving this interaction towards ferromagnetism. Although this compound contains considerable local polarity resulting from SeO_3 polyhedra and distorted VO_6 octahedra these polarisations are not aligned in the structure and so only weak second harmonic generation is seen. The ferroborate $K_2Fe_2B_2O_7$ crystallises in the noncentrosymmetric space group P321 and demonstrates substantially larger second harmonic generation to give a maximum value of *ca.* 0.4 times that of potassium dihydrogen phosphate.[22] The compound adopts a layered structure built up from BO_3 trigonal planar units and FeO_4 tetrahedra as shown in Fig. 5. The three crystallographically distinct Fe^{2+} cations are distributed over a triangular lattice and this frustrates the

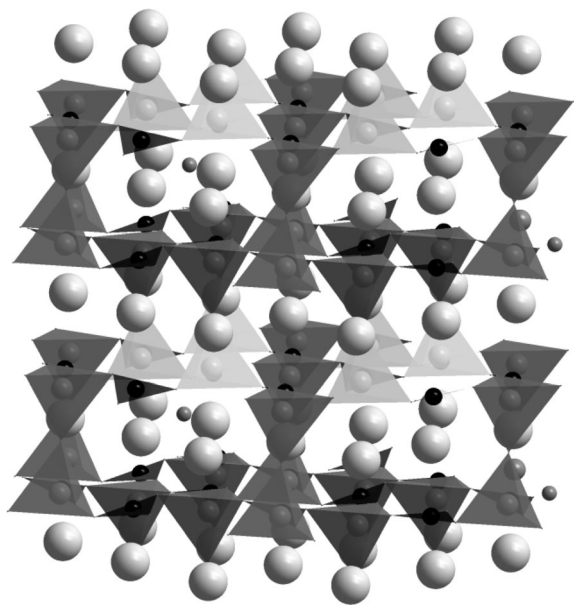

Fig. 5 The crystal structure of $K_2Fe_2B_2O_7$ is composed of a corner-linked network of FeO_4 and BO_3 units represented by tetrahedral and trigonal planar units respectively. Large grey spheres represent K^+ cations.[22]

antiferromagnetic interactions leading to the probable formation of a spin glass state below a magnetic transition temperature of 20 K.

Hydrothermal synthesis has produced a new open framework iron phosphate, $(NH_4)_4Fe_3(OH)_2F_2[H_3(PO_4)_4]$.[23] This is built up from a novel trimer of corner-linked FeO_6 octahedra that are themselves linked by phosphate groups to give a three-dimensional structure that contains ten-member rings that enclose one-dimensional channels that accommodate the ammonium cations. This compound undergoes a magnetic transition at 17 K that leads to the spin cancellation associated with either antiferromagnetism or spin glass behaviour. The large Weiss constant of −187 K indicates that the strong antiferromagnetic interactions are substantially frustrated in this structure.

An detailed study of $(MoO_2)_2P_2O_7$ has identified a previously unobserved phase in this system and found that the room temperature structure is more complex than previously reported.[24] At 423 K the γ-phase forms in Pnma and contains two crystallographically distinct Mo sites and two crystallographic P positions to give a network composed of MoO_6 and PO_4 units. On cooling, this phase undergoes a transition at 377 K to form an incommensurate phase which transforms to a commensurate phase on cooling further to 325 K. The structure of this low temperature α-$(MoO_2)_2P_2O_7$ phase is indicated by exceedingly weak superstructure peaks in the X-ray- and neutron- powder diffraction profiles that required a much more complex description of the structure in space group $P2_1/c$ with eight Mo-, eight P- and 44 O atoms in the asymmetric unit. It is thought that the complexity of the low temperature structure is a result of balancing the requirements of the local coordination environment with the longer-range constraints imposed by the connectivity of the structure. A series of sequential transitions have also been observed in the dehydration of $MoO_2PO_3OH{\cdot}H_2O$ to form γ-$(MoO_2)P_2O_7$ leading to the identification of two new phases.[25] β-$MoOPO_4$ is formed by complete dehydration of the starting material and has a three-dimensional structure where all MoO_6 and PO_4 units are fully corner linked. Careful control of heating rate during the dehydration led to the formation of δ-$MoOPO_4$ which contains layers built up from chains of MoO_6 which are linked by PO_4 groups. This layered phase is capable of accommodating Li^+ which is reductively intercalated between the layers leading to a modest increase in the unit cell volume.

Immersion of $Na_3MnH(P_{0.4}O_4)_2$ in an aqueous solution containing Cs^+ leads to the formation of a new compound $CsMn(PO_4){\cdot}6H_2O$.[26] This layered structure contains MnO_6 octahedra and PO_4 tetrahedra and forms an unusual structure that does not resemble any known transition metal phosphates but does have similarities with $CsMg(OH_2)_6(PO_4)$. The structure contains a three-layer repeat composed of $[PO_4]^{3+}$, $[Mn(H_2O)_6]^{2+}$ and Cs^+. The caesium cations are in a distorted cubo-octahedral environment and bond valence sums suggest that they are significantly underbonded with a mean Cs–O bond length of 3.92 Å. The framework shows considerable selectivity for Cs^+ over other Group 1 cations and it is thought that this arises from the unique ability of Cs^+ to drive recrystallisation of the product after dissolution of the initial framework.

A number of new beryllosilicate framework materials have been prepared for the first time including a compound that has the structure of zeolite nabesite.[27] Nabesite has only been observed at a single geological site, in South Greenland, and hydrothermal methods have been used to in the first synthesis of compounds with this structure, $Na_{5.28}[Be_{2.64}Si_{17.36}O_{40}]{\cdot}12.5H_2O$ and $K_8[Be_4Si_{16}O_{40}]{\cdot}12H_2O$. These compounds contain an ordered arrangement of SiO_4 and BeO_4 tetrahedra although

with a degree of chemical disorder resulting from a lower beryllium content than that found in mineral samples. These tetrahedra form sheets which are linked by BeO_4 units to give a three dimensional network containing channels capable of accommodating Na^+ or K^+ cations at different sites reflecting the different cation sizes. A wide range of other framework beryllosilicates have also been reported including layered phases and a number of analogues of aluminosilicate zeolites. The incorporation of Be^{2+} into these frameworks instead of Al^{3+} offers a route to materials with considerably lower density which could be highly advantageous in gas storage applications as long as the hazards due to the toxicity of beryllium are minimised. The naturally occurring phase $BaB_2Si_2O_8$ has also been synthesised for the first time and has been use as a host lattice to study the photoluminescence of Eu^{3+} and Tb^{3+}.[28] Ba^{2+} is ten-coordinate and B^{3+} and Si^{4+} are both found in heavily distorted tetrahedral that are linked *via* corner-sharing. The introduction of 0.01 Eu per formula unit into the parent compound, or the Sr^+ analogue, gives red emission, or blue if introduced into the $SrB_2Si_2O_8$ lattice. This arises due to partial reduction of Eu^{3+} to Eu^{2+} at high temperatures.

3. Nitrides, chalcogenides and halides

These compounds provide a diverse range of properties that include many attributes observed in oxides, but more interestingly give access to structures and properties that have not previously been observed. A new complex sulphide has been reported that shoes a range of unusual properties that combine to allow it to give remarkable ion exchange properties. $[(CH_3)_xNH_2]_2Ga_2Sb_2Sb_7{\cdot}H_2O$ crystallises in the non-centrosymmetric space group $P2_1$ and contains layers of composition $[Ga_2Sb_2S_7]^{2-}$ which are linked *via* hydrogen bonding by the dimethylammonium cations.[2] The layers contain holes which are stacked above each other to give channels with dimensions of *ca.* 2.8 × 7.6 $Å^2$ that give highly selective ion exchange. The dimethylammonium cation can be exchanged for Cs^+ selectively over other alkali metals. Rubidium is the only other Group 1 metal that is absorbed into the structure, and exposure of the as-made material to an equimolar mixture of Na^+, K^+, Rb^+, Cs^+ and Sr^{2+} showed that an order of magnitude more Cs^+ was exchanged than Rb^+. None of the other cations were inserted into the material at a detectable level. Structural characterisation of the Cs^+-containing material showed that this selectivity arises from a structural rearrangement around this cation closing the window and rendering the structure impermeable. This is described as a Venus flytrap action.

The thermoelectric properties of Bi_2Te_3 mean that it has been widely studied. Doping this compound with small amounts of manganese has been used to induce ferromagnetism in the series $Bi_{2-x}Mn_xTe_3$ with a Curie temperature of *ca.* 10 K being developed in materials containing only $x = 0.04$ manganese.[29] For more dilute doping levels there is no ferromagnetic transition and the high temperature paramagnetic behaviour indicates only very weak coupling between magnetic moments. Increasing the doping level shows that for $Bi_{1.96}Mn_{0.04}Te_3$ and $Bi_{1.91}Mn_{0.09}Te_3$ the magnetic interactions are considerably stronger and the Weiss constants of 11 K and 13 K respectively provide excellent agreement with the observed ferromagnetic transition temperatures. Careful measurements on a single crystal show that the manganese atoms are evenly distributed in the lattice and show that this material is a dilute ferromagnetic semiconductor and that the behaviour does not arise from clustering effects.

Two new isostructural oxyselenide compounds have been found that contain complex layered structures.[30] $La_2O_2MnSe_2$ and $La_2O_2FeSe_2$ contain sheets composed of chains of edge-shared MSe_4O_2 octahedra linked to partially disordered MSe_4 tetrahedra. These sheets are bridged by ribbons of La_2O_2Se that contain La_4O tetrahedral units. $La_2O_2MnSe_2$ undergoes a reversible phase transition at *ca.* 255 K related to ordering of the tetrahedrally-coordinated manganese. Both compounds show localised electronic behaviour with antiferromagnetic ordering occurring at low temperature and electronic band gaps of 1.6 eV and 0.7 eV for $La_2O_2MnSe_2$ and $La_2O_2FeSe_2$ respectively. The stoichiometrically related compound $La_2O_3Mn_2Se_2$ adopts a very different structure with sheets of La_4O tetrahedra alternating with sheets made up of face-sharing $MnSe_4O_2$ octahedra.[31] The latter results in a square lattice of magnetic ions that is similar to the pnictide superconductors. This lattice allows two-dimensional magnetic order to persist at the relatively high temperature of 350 K albeit over a length scale of only three unit cells. The layered nature of the structure inhibits the formation of a three-dimensionally ordered magnetic phase and long-range antiferromagnetic ordering is only observed below a Neel temperature of 163 K.

The use of a calcium chloride flux in the attempted synthesis of a mixed metal oxide has fortuitously led to the formation of a series of new complex oxychlorides, $Ca_4Fe_{3-x}Mn_xO_{8-\delta}Cl_2$.[32] These tetragonal phases adopt the $n = 3$ Ruddlesden Popper structure with a double layer of perovskite $Ca_3Fe_{3-x}Mn_xO_{8-\delta}Cl$ separated by a single layer of rock salt CaCl as shown in Fig. 6. The chloride ions in the perovskite block are found in the sites adjacent to the rock salt layer and this results in the central transition metal cation in the perovskite block being coordinated by six oxide anions, whilst the other two metals are octahedrally coordinated by five oxides and a chloride. There is considerable positional disorder in the anions of the perovskite and although this is not ordered and does not violate the tetragonal symmetry, Mössbauer spectra show that the iron distribution is more complex that suggested by the presence of only two crystallographically-distinct sites for this cation. There is strong antiferromagnetic coupling between the transition metal cations in these phases at room temperature, but this fails to form an antiferromagnetically ordered phase presumably as a result of occupational and positional disorder leading to frustration and spin glass behaviour.

The one-dimensional structure of the oxychloride $Ba_8Co_2Mn_6ClO_{22}$ has been investigated using a wide-range of techniques to understand the factors that stabilise this unusual structure.[33] This compound contains chains of six face-sharing MnO_6 octahedra linked *via* corner-sharing by CoO_3Cl tetrahedra. This is the first observation of six member chains of face-sharing octahedra and it is thought that this is stabilised by the chemical ordering of cobalt and manganese over the octahedrally- and tetrahedrally-coordinated sites.

A novel application of ionic liquids as solvents for chalcogenides has led to the formation of $[Bi_2Te_2Br](AlCl_4)$.[34] Dissolution of bismuth and tellurium in elemental form in 1-ethyl-3-methylimidazolium aluminium chloride at 165 °C led to reaction between the metals and the ionic liquid and the formation of a structure composed of positively charged layers $[Bi_2Te_2Br]^+$ separated by $[AlCl_4]^-$ anions. This structure leads to highly anisotropic band structure with electrical conductivity parallel to the layers being six orders of magnitude larger than perpendicular to the layers due to the $[AlCl_4]^-$ units effectively blocking the passage of charge. The layered pnictides LiFeP and LiCuP have been known for several decades, but their low temperature properties have been studied in detail for the first time.[35] This has revealed the

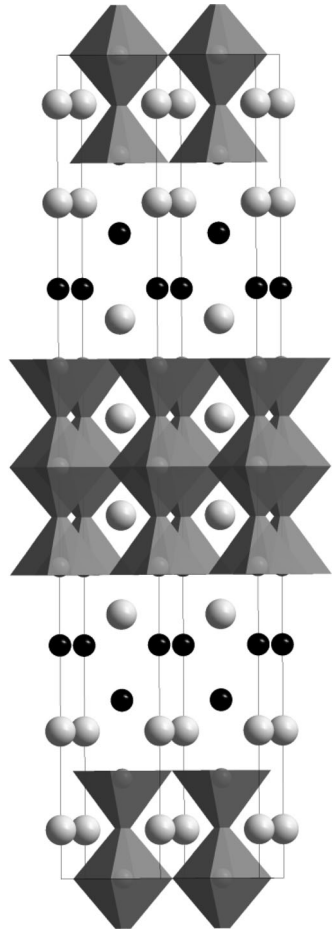

Fig. 6 The $n = 3$ Ruddlesden Popper structure of the oxychloride phases $Ca_4Fe_{3-x}Mn_xO_{8-\delta}Cl_2$. Disorder in the oxide positions has been omitted for clarity. Shaded polyhedra indicate the coordination environment around the Fe/Mn cations. Light grey and black spheres represent Ca^{2+} and Cl^- respectively.[32]

presence of superconducting transitions at 3.7 K and 4.1 K for LiFeP and LiCuP respectively. These compounds adopt similar structures to the iron-based pnictides that show superconductivity at temperatures up to 55 K. These observations suggest a range of doping studies to examine whether the structural drivers of superconductivity in the iron phases recur in LiFeP and LiCuP.

Reductive nitridation of metal oxides and nitrates has led to the formation of a number of isostructural complex metal nitrides $M_2M'Mo_3N$ where M and M' are various combinations of Ni, Co, Ge, Ga or Fe.[36] These compounds all adopt the η-carbide structure and show metallic conductivity. The magnetic behaviour varies considerably with no long-range magnetic order occurring in the series $Ni_{2-x}Co_xGeMo_3N$, but the closely related composition $Co_2Ge_{0.3}Ga_{0.7}Mo_3N$ adopts a long range antiferromagnetically-ordered phase below 90 K. Low temperature neutron diffraction experiments showed that the observed spin cancellation arises from antiferromagnetic coupling of ferromagnetically-coupled Co_4 clusters.

Growth of $LaTiO_2N$ by an unusual flux method has stabilised a form of this compound in a space group, Imma, that has not previously been observed for a perovskite oxynitride.[37] The nitride and oxide anions are randomly distributed over the two crystallographic sites in the structure and the presence of nitride gives a reduced band gap resulting in a red colour and the potential for photocatalytic activity using visible light. The mixed oxynitrides $Ln_3[SiON_3]O$ adopt structures that are related to the *anti*-perovskite structure with a framework composed of corner-sharing Ln_6O octahedral.[38] The interstices in the structure are occupied by SiO_3N tetrahedral and these units appear to impart considerable reactivity on these compounds; these phases are sensitive to air and water whereas analogous compounds where the interstitial species are bonded to the framework are relatively inert and stable.

4. Intermetallic compounds

Careful control of synthetic conditions has allowed the preparation of the face-centred cubic (*fcc*) polymorph of Cs_3C_{60} in samples containing minimal amounts of the more stable body-centred cubic polymorph.[1] This has allowed comparison of the effects of different packing arrangements of the C_{60}^{3-} units on the electronic properties to be made. The *fcc* polymorph of Cs_3C_{60} is unique amongst face centred fullerides in that it is not superconducting under ambient pressure but instead orders antiferromagnetically at 2.2 K. The application of pressure induces bulk superconductivity at 2.2 kbar and drives the transition temperature to a maximum value of 35 K that is only slightly lower than the 38 K observed in the body-centred cubic polymorph. Comparison of the behaviour of these two polymorphs shows that the superconducting transition temperature scales with the proximity to the metal-insulator transition and is independent of the type of lattice.

A new structure has been identified in an antimonide, $Hf_3Cu_2Ge_{3.58}Sb_{1.42}$, produced by heating an ingot of hafnium, copper and germanium under vacuum with antimony.[39] The structure can be considered to be built up from layers of structure types ZrSiS and $NdTe_3$. It appears that the occupational disorder between Ge and Sb is a key component in stabilising this structure as it provides an entropic term that is otherwise absent. Despite this disorder, the compound is metallic and band structure calculations show that this metallic character is independent of what fraction of germanium and antimony is used in the simulation. Mixed cation site occupancy is also crucial to the formation of two new phases $A_5In_3Ge_6$ where A is a mixture of either Ca and Sr or Eu and Yb.[40] These compounds adopt a new structure type containing a negatively charged framework made up of chains of corner-shared $InGe_4$ tetrahedra that are linked by Ge_4 units and $InGe_4$ square planes. The cations occupy a range of extra-framework sites with considerable occupational disorder. This description may suggest a weak coupling between the cations and the framework, but band structure calculations show that there is a substantial contribution from the Sr 5s and Ca 4s orbitals to the bands close to the Fermi level.

A new antimonide Ba_2ZnSb_2 has been reported, along with isostructural arsenic and bismuth analogues.[41] This Zintl phase contains novel one-dimensional structures built up from edge-sharing $ZnSb_4$ tetrahedra as shown in Fig. 7. These chains are separated by Ba^{2+} cations which are octahedrally-coordinated to six antimony atoms with four zinc cations at a relatively short distance, but with no bonding interaction between the Ba-Zn atom pair.

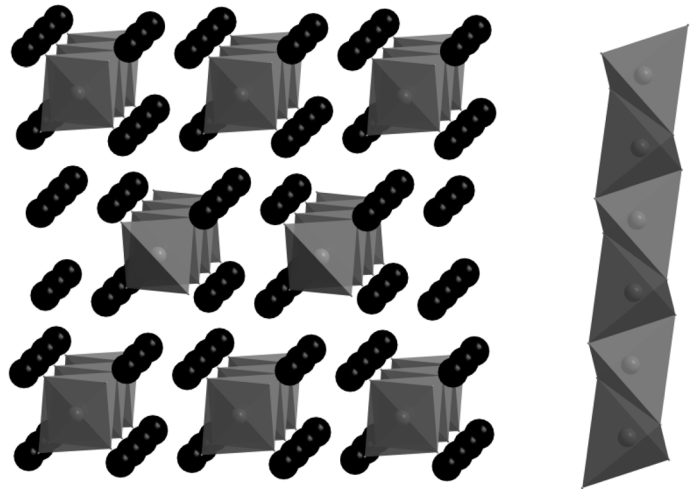

Fig. 7 The isostructural compounds Ba_2ZnPn_2 (*Pn* = As, Sb, Bi) contain chains of edge-sharing $ZnPn_4$ tetrahedra running along the *z*-direction. Black spheres represent the Ba^{2+} cations.[41]

References

1 A. Y. Ganin, Y. Takabayashi, P. Jeglic, D. Arcon, A. Potocnik, P. J. Baker, Y. Ohishi, M. T. McDonald, M. D. Tzirakis, A. McLennan, G. R. Darling, M. Takata, M. J. Rosseinsky and K. Prassides, *Nature*, 2010, **466**, 221.
2 N. Ding and M. G. Kanatzidis, *Nat. Chem.*, 2010, **2**, 187.
3 K. E. Johnston, C. C. Tang, J. E. Parker, K. S. Knight, P. Lightfoot and S. E. Ashbrook, *J. Am. Chem. Soc.*, 2010, **132**, 8732.
4 C. H. Hervoches and C. Greaves, *J. Mater. Chem.*, 2010, **20**, 6759.
5 F. Ramezanipour, J. E. Greedan, A. P. Grosvenor, J. F. Britten, L. M. D. Cranswick and V. O. Garlea, *Chem. Mater.*, 2010, **22**, 6008.
6 J. Seddon, E. Suard and M. A. Hayward, *J. Am. Chem. Soc.*, 2010, **132**, 2802.
7 C. He, X. Z. Li, Z. J. Wang, X. F. Long, S. Y. Mao and Z. G. Ye, *Chem. Mater.*, 2010, **22**, 5588.
8 S. H. Kim, P. S. Halasyamani, B. C. Melot, R. Seshadri, M. A. Green, A. S. Sefat and D. Mandrus, *Chem. Mater.*, 2010, **22**, 5074.
9 A. Yamamoto, D. Hashizume, H. A. Katori, T. Sasaki, E. Ohmichi, T. Nishizaki, N. Kobayashi and H. Takagi, *Chem. Mater.*, 2010, **22**, 5712.
10 S. J. Mugavero III, A. H. Fox, M. D. Smith and H.-C. zur Loye, *J. Solid State Chem.*, 2010, **183**, 465.
11 H. El Shinawi and C. Greaves, *J. Mater. Chem.*, 2010, **20**, 504.
12 H. El Shinawi, A. Bertha, J. Hadermann, T. Herranz, B. Santos, J. F. Marco, F. J. Berry and C. Greaves, *J. Solid State Chem.*, 2010, **183**, 1347.
13 Y. Tsujimoto, A. Kitada, Y. J. Uemura, T. Goko, A. A. Aczel, T. J. Williams, G. M. Luke, Y. Narumi, K. Kindo, M. Nishi, Y. Ajiro, K. Yoshimura and H. Kageyama, *Chem. Mater.*, 2010, **22**, 4625.
14 M. J. Martinez-Lope, J. A. Alonso, D. Sheptyakov and V. Pomjakushin, *J. Solid State Chem.*, 2010, **183**, 2974.
15 A. R. Armstrong, C. Arrouvel, V. Gentili, S. C. Parker, M. S. Islam and P. G. Bruce, *Chem. Mater.*, 2010, **22**, 6426.
16 I. P. Roof, M. D. Smith and H. C. zur Loye, *Solid State Sci.*, 2010, **12**, 759.
17 H. V. Goulding, S. E. Hulse, W. Clegg, R. W. Harrington, H. Y. Playford, R. I. Walton and A. M. Fogg, *J. Am. Chem. Soc.*, 2010, **132**, 13618.
18 J. B. Liang, R. Z. Ma, F. X. Geng, Y. Ebina and T. Sasaki, *Chem. Mater.*, 2010, **22**, 6001.
19 J. B. Liang, R. Z. Ma, N. B. O. Iyi, Y. Ebina, K. Takada and T. Sasaki, *Chem. Mater.*, 2010, **22**, 371.

20 S. Vilminot, P. J. Baker, S. J. Blundell, T. Sugano, G. Andre and M. Kurmoo, *Chem. Mater.*, 2010, **22**, 4090.
21 S. H. Kim, J. Yeon, A. S. Sefat, D. G. Mandrus and P. S. Halasyamani, *Chem. Mater.*, 2010, **22**, 6665.
22 Y. Wang and R. K. Li, *J. Solid State Chem.*, 2010, **183**, 1221.
23 J. X. Mi, C. X. Wang, N. Chen, R. Li and Y. M. Pan, *J. Solid State Chem.*, **183**, 2763.
24 S. E. Lister, A. Soleilhavoup, R. L. Withers, P. Hodgkinson and J. S. O. Evans, *Inorg. Chem.*, 2010, **49**, 2290.
25 S. E. Lister, V. J. Rixom and J. S. O. Evans, *Chem. Mater.*, 2010, **22**, 5279.
26 S. Ferdov and Z. Lin, *Chem. Mater.*, 2010, **22**, 5345.
27 J. A. Armstrong and M. T. Weller, *J. Am. Chem. Soc.*, 2010, **132**, 15679.
28 M. P. Saradhi, S. Boudin, U. V. Varadaraju and B. Raveau, *J. Solid State Chem.*, 2010, **183**, 2496.
29 Y. S. Hor, P. Roushan, H. Beidenkopf, J. Seo, D. Qu, J. G. Checkelsky, L. A. Wray, D. Hsieh, Y. Xia, S. Y. Xu, D. Qian, M. Z. Hasan, N. P. Ong, A. Yazdani and R. J. Cava, *Phys. Rev. B: Condens. Matter Mater. Phys.*, 2010, **81**, 7.
30 E. E. McCabe, D. G. Free, B. G. Mendis, J. S. Higgins and J. S. O. Evans, *Chem. Mater.*, 2010, **22**, 6171.
31 N. Ni, E. Climent-Pascual, S. Jia, Q. Huang and R. J. Cava, *Phys. Rev. B: Condens. Matter Mater. Phys.*, 2010, 214419.
32 T. Yang, J. Sun, M. Croft, I. Nowik, A. Ignatov, R. Cong and M. Greenblatt, *J. Solid State Chem.*, 2010, **183**, 1215.
33 M. Iorgulescu, H. Kabbour, N. Tancret, O. Mentre and P. Roussel, *Chem. Commun.*, 2010, **46**, 5271.
34 K. Biswas, Q. Zhang, I. Chung, J.-H. Song, J. Androulakis, A. J. Freeman and M. G. Kanatzidis, *J. Am. Chem. Soc.*, 2010, **132**, 14760.
35 J. T. Han, J. S. Zhou, J. G. Cheng and J. B. Goodenough, *J. Am. Chem. Soc.*, 2010, **132**, 908.
36 L. A. Sviridov, P. D. Battle, F. Grandjean, G. J. Long and T. J. Prior, *Inorg. Chem.*, 2010, **49**, 1133.
37 M. Yashima, M. Saito, H. Nakano, T. Takata, K. Ogisu and K. Domen, *Chem. Commun.*, 2010, **46**, 4704.
38 J. A. Kechele, C. Schmolke, S. Lupart and W. Schnick, *Z. Anorg. Allg. Chem.*, 2010, **636**, 176.
39 M. Guch, C. R. Sankar, A. Assoud and H. Kleinke, *Chem. Mater.*, 2010, **22**, 6433.
40 T.-S. You and S. Bobev, *J. Solid State Chem.*, 2010, **183**, 1258.
41 B. Saparov and S. Bobev, *Inorg. Chem.*, 2010, **49**, 5173.